Morphological-Based Filtering of Noise: Practical Study on Solar Images

M. Al-Omari, R. Qahwaji, T. Colak, and S. Ipson
School of Informatics, Department of Electronic Imaging and Media Communications,
University of Bradford, Bradford BD7 1DP, UK
(e-mails: m.h.al-omari@brad.ac.uk, r.s.r.qahwaji@brad.ac.uk, t.colak@brad.ac.uk, s.s.ipson@brad.ac.uk)

Abstract— ***In this paper, a morphological-based algorithm is proposed for noise filtering in digital images. This algorithm is based on the morphological hit-miss transform (HMT). It is applied on a real-life problem, which is the detection of solar features in H-alpha solar images that are obtained from Meudon Observatory. These images are processed by the automated detection system of Filaments reported by R. Qahwaji and T. Colak [1]. The automated detection system works well when detecting filaments in noise-free solar images; it achieves false acceptance rate (FAR) error rate of 4% and false rejection rate (FRR) error rate of 36% when compared with the manually detected filaments in the synoptic maps. When the detection is applied after the addition of Gaussian noise to the solar images it achieves FAR of 3% and FRR of 51%. Then by filtering using the proposed algorithm, the detection performance is enhanced to achieve FAR of 8% and FRR of 13%.***

***Index Terms*—image processing; solar imaging; morphology; hit-miss transform; noise; Filtering**

1. Introduction

By definition, Noise is random fluctuations in intensity values that affects image content, and it usually occurs during image capture, transmission or processing [2]. Some of the common noise types are salt and pepper noise, impulse noise and Gaussian noise. Impulse noise, together with salt and pepper noise occur at random locations in the image, while all image pixels are affected by Gaussian noise [3]. The noise pattern in solar images is generally shot noise with Poisson distribution but it can be approximated by additive Gaussian noise for large numbers of electron emissions [4]. This noise comes from the quantum nature of light and the uncertainty in the number of electrons emitted by a photo detector.

In this paper, a morphological algorithm that is used to filter noise in digital images is designed and tested with the detection system introduced in [1]. The proposed algorithm can be implemented as a pre-processing step for many real-life applications.

The Detection of solar features is very important because of their direct relation to space weather activities. The term "space weather" refers to adverse conditions on the Sun, in the solar wind, and in the Earth's magnetosphere, ionosphere, and thermosphere that may affect space-borne or ground-based technological systems and can endanger human health or life [5]. Space weather is of great importance to many modern technologies and like ordinary weather, it produces low-level effects on human technology; interspersed with occasional dramatic events.

This paper is organized as follows: in section 2, a brief survey on noise filtering is presented. In section 3, the design of the proposed morphological filter is discussed. Section 4 provides information about the solar images used in this article. In section 5 the noise simulation for solar Images is discussed. A practical application on the filtering of solar images is presented in section 6. And the performance of the proposed filtering algorithm is tested in section 7. This paper ends with a conclusions section.

2. Brief survey on filtering

The noise-removal process can be carried out using non-linear Laplacian filters. However, the filtering process depends on the accurate determination of its threshold and there are no agreed upon methods for determining the optimum thresholds [6]. A traditional technique for detecting the regions of interest (ROI) is to apply a pre-processing stage to filter-out the noise before implementing the segmentation and/or the feature extraction stages. In [7], the Fast Fourier Transform (FFT) is applied to remove periodic background noise patterns that have high spatial frequencies before applying the edge detection to coastal thematic mapper images. However, this process is not fully automated and user interaction is required. Signal-Dependent Rank Order Mean Filter (SD-ROM) is a decision-based filter that classifies every processed pixel as either being corrupted or uncorrupted by estimating the noise level [2]. SD-ROM is an alternative to median filters but it is mainly applied for the filtering of impulse noise. The SD-ROM orders the pixel values in the mask window in an ascending order. All the distances in the 3×3 mask between the ordered elements and the central pixel are ciphered and used later to replace the central pixel if any of the distances exceed the thresholds. The selection of the thresholds involves a balance between the number of detected impulses and the number of removed image details [8, 9].

3. Design of the morphological filter

The theory of mathematical morphology consists of image transformations that are based on set-theoretical, geometrical and topological concepts [10]. Mathematical morphology is useful for the analysis of

geometrical structures in images [11], the reduction of clutter in images, image enhancement and segmentation of ROI [12]. It is used widely in image analysis (i.e. edge detection, shape analysis, image coding, smoothing and thinning) [13].

The hit-miss transform was introduced by Casasent et al in [14, 15]. Many steps are involved in implementing the morphological Hit-Miss Transform (HMT). The transform starts by converting the grey-scale image to a binary image. This process is one of the challenges the HMT faces, and may be the main cause behind any shape distortions. An important question is "how to determine the threshold value?" A suggested solution is to use an "above the mean" threshold [14-16]. This method may lead to inaccurate description, especially when the objects contained in the image are of different nature (i.e., some parts of the image contain bright objects while other parts contain dark objects) [16, 17].

The hit-miss transform (HMT) of binary image X with hit structuring element H and miss structuring element M produces image $Z = (X \Theta H) \cap (X^c \Theta M)$ [2], where X^c is the complement of the binary image X, Θ represents the correlation operation and $\cap$ represents the AND operation.

For this work, we have defined a HMT that uses a single mask to carry out the hit and miss operations. The new mask is shown in Fig. 1. The hit structuring element of the filter is represented by 1, the miss structuring element is represented by -1 and the zeros indicate pixels to be ignored.

-1	-1	-1	-1	0	0	0	0	0	0	0	0	-1	-1	-1	-1
-1	-1	-1	-1	0	0	0	0	0	0	0	0	-1	-1	-1	-1
-1	-1	-1	-1	0	0	0	0	0	0	0	0	-1	-1	-1	-1
-1	-1	-1	-1	0	0	0	0	0	0	0	0	-1	-1	-1	-1
0	0	0	0	1	1	1	1	1	1	1	1	0	0	0	0
0	0	0	0	1	1	1	1	1	1	1	1	0	0	0	0
0	0	0	0	1	1	1	1	1	1	1	1	0	0	0	0
0	0	0	0	1	1	1	1	1	1	1	1	0	0	0	0
0	0	0	0	1	1	1	1	1	1	1	1	0	0	0	0
0	0	0	0	1	1	1	1	1	1	1	1	0	0	0	0
0	0	0	0	1	1	1	1	1	1	1	1	0	0	0	0
0	0	0	0	1	1	1	1	1	1	1	1	0	0	0	0
-1	-1	-1	-1	0	0	0	0	0	0	0	0	-1	-1	-1	-1
-1	-1	-1	-1	0	0	0	0	0	0	0	0	-1	-1	-1	-1
-1	-1	-1	-1	0	0	0	0	0	0	0	0	-1	-1	-1	-1
-1	-1	-1	-1	0	0	0	0	0	0	0	0	-1	-1	-1	-1

Figure 1 Hit-Miss Filter

The hit-miss operation is carried out by correlating the mask of Fig. 1 with the input image and comparing the outcomes of correlation for the hit process and the miss process. If the absolute energy of the hit process is smaller than that of the miss process then the central pixel is highlighted as a region of interest or a foreground object. Otherwise, the central pixel is replaced with a constant gray level representing the background.

4. H-alpha Images

A H-alpha images, which is shown in (Fig. 2), is captured by observing light from a particular line in the hydrogen spectrum at 6563 Å (red light) [18]. The core of the line is formed between 1200 and 1800 km above the visible surface. The presence of interacting magnetic fields in the chromosphere generates an enormous amount of heat. The heated regions are represented by brighter pixels in the captured H-alpha images. H-alpha images also show many dark filamentary structures on the solar disk, which correspond to magnetic loops reaching up into the solar corona. These features tend to be cooler than the surrounding corona and permit H-alpha absorption to take place, hence their dark appearance [19].

Full disk images of the Sun at the H-alpha wavelength have been made from the ground since 1926. In this paper, H-alpha images are obtained from Meudon observatory-France http://bass2000.obspm.fr. Satellites can be used to capture these images and this would achieve near 100% temporal coverage [20]. H-alpha images are used for examining chromospheric features like filaments sunspots, and flares.

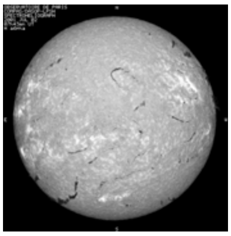

Figure 2 A H-α image captured on July 2, 2001 by Meudon bservatory.

5. Noise simulation in solar Images

Solar images are affected by different levels of noise. The noise level increases in times of high solar activities. According to [4], this noise can be simulated using Gaussian noise with the mean set equal to 40% of the image mean and the standard deviation set equal to 10. We have used these values to simulate solar noise in this work. The noisy version of Fig. 2 is shown in Fig. 3.a. The Filtering process, as explained in Section 3, is applied to this noisy image and the result is shown in Fig. 3.b.

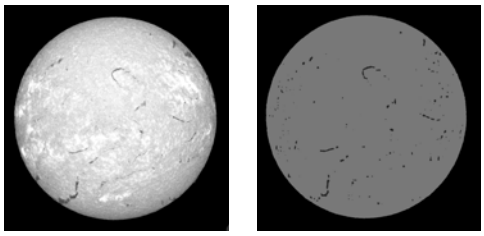

(a) Noisy solar image (b) Filtered image

Figure 3 Noise Simulation and Filtering

6. Practical implementation on solar images

In [1], a hybrid system for the automatic detection and verification of solar features in H-alpha and CaKIII images is introduced. This hybrid system consists of several imaging and machine learning stages. In the first stage the solar disk is detected using the morphological HMT, watershed transform and the Filling algorithm. To remove the limb-darkening effect, this system introduces an image-enhancement

technique. Afterwards, intensity filtering is applied which is followed by a modified region-growing technique to detect the regions of interest (RoI) such as filaments. Statistical feature extraction and neural networks are applied next to verify the detected features and enhance the detection performance.

The original image of Fig. 4.a is used as input to the detection system and the result is depicted in Fig. 4.b which can be compared with the manually detected filaments in the Synoptic map of Fig. 4.c. the Synoptic maps are publicly available from Meudon's observatory website at (http://bass2000.obspm.fr).

To simulate real-life noise affecting these images, Gaussian noise with a mean value equal to 40% of the image mean and a standard deviation value of 10 is added to all the images in the test set. Fig. 4.d. shows the original image of Fig. 4.a. after adding noise to it. Applying the algorithm of [1] to this image provides the image shown in Fig. 4.e. Applying the morphological filtering algorithm explained earlier to the noisy image before applying the algorithm of [1] produces the image shown in Fig. 4.f.

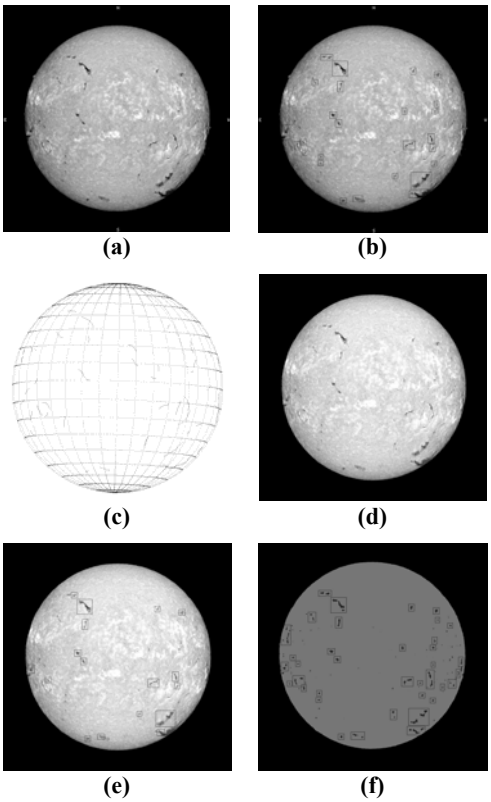

Figure 4 The detection of filaments (a) Original image (b) Detection of filaments for the original image (c) Synoptic Map for Filaments from Meudon (d) Original image with Gaussian noise of mean equals 40% of the image mean (e) Detection for the noisy image (f) Detection for the filtered noisy image.

7. Testing the filtering process with filaments detection

The features detection system of [1] is applied on Meudon's H-alpha images for the detection of filaments. The performance of [1] is analyzed further by adding noise, as explained before, to these images and then applying the detection algorithm again. Images covering the period from July 2, 2001 till August 4, 2001 are used.

The results for the detection of filaments are shown in Table 1. The first column shows the date for each H-α image, while the total number of filaments that are manually detected is indicated in the second column. The False Acceptance Rate (FAR) and the False Rejection Rate (FRR) are calculated as explained in [1] and are shown in Table 1. The FAR error rate represents the percentage of the detected ROI that do not contain real filaments. On the other hand, the FRR error rate is the percentage of the filaments that are not detected in the resulting image.

Table 1 FAR% and FRR% for filaments detection

Date	Filaments	Detection for the original images		Detection for the noisy images		Detection for the filtered noisy images	
		FAR %	FRR %	FAR %	FRR %	FAR %	FRR %
02/07	56	4	41	4	64	7	24
03/07	54	2	37	0	56	6	26
04/07	49	0	44	0	54	2	17
06/07	55	0	31	0	48	8	12
09/07	47	5	42	3	54	8	20
10/07	43	0	40	0	62	2	15
11/07	37	7	26	0	38	16	3
15/07	33	6	34	7	46	14	9
16/07	30	10	38	4	44	17	3
17/07	39	5	32	4	53	8	24
19/07	46	9	29	6	49	17	2
20/07	42	8	45	4	61	8	9
21/07	41	10	44	6	51	2	14
22/07	47	4	32	5	42	15	8
24/07	59	2	51	3	64	3	14
25/07	41	6	44	3	51	2	9
27/07	49	2	31	0	48	2	12
29/07	43	5	44	0	57	4	18
30/07	51	2	15	0	35	11	11
31/07	53	3	25	4	45	11	2
03/08	51	3	26	2	46	6	17
04/08	42	0	38	0	50	8	20
Average	46	4	36	3	51	8	13

The results of Fig. 5 show that the filtering stage reduces the average FRR error rate compared to the FRR for non-noisy images. This proves that our algorithm is a good pre-processing tool. The FAR is slightly higher than the original FAR. We believe this is caused by the verification stage of detected regions which is carried out by neural networks. Statistical features belonging to non-noisy samples were only considered. The performance may improve if noisy features are also considered in the training of neural networks.

8. Conclusions

In this paper, we propose a morphological-based filtering algorithm. A new hit-miss transform that uses a single filter is introduced in this work. A single filter detects the hit regions and detects at the same time the miss regions. The energies of both regions are compared to determine whether the central pixel belongs to the regions of interest or not. The

morphological filter introduced here is used as a filtering algorithm to filter noise in digital images.

Our algorithm is tested on H-alpha images that are obtained from the Meudon Observatory, covering the period from July 2, 2001 till August 4, 2001. The detection of filaments for noise-free H-alpha images achieves a FAR error rate of 4% and a FRR error rate of 36%, when compared with the manually detected filaments in the corresponding synoptic maps. The detection for noisy images achieves a FAR error rate of 3% and a FRR error rate of 51%, which has been enhanced by filtering to achieve a FAR error rate of 8% and a FRR error rate of 13%.

For the future, we would like to introduce a morphological-based filtering system that can be used to filter different types of noise and for different applications (i.e. solar imaging, remote sensing and mammography, etc.).

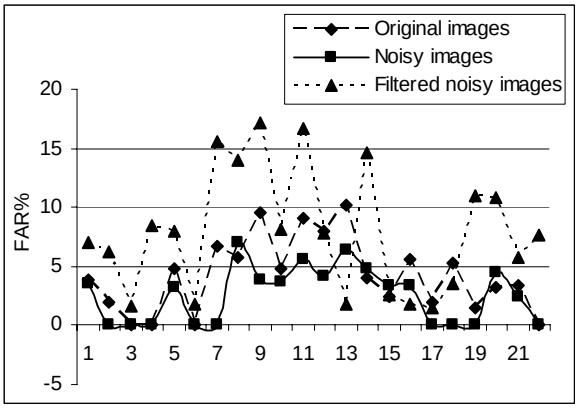

(a) FAR%

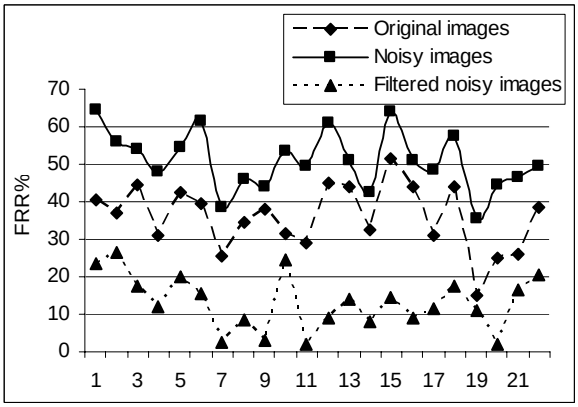

(b) FRR%

Figure 5 FAR% and FRR% for filaments detection

References

[1] R. Qahwaji and T. Colak, "Automatic Detection and Verification of Solar Features," *Wiley Periodicals, Inc.*, vol. 15, pp. 199-210, 2005.

[2] R. Qahwaji, "Detecting Edges in Noisy Face Database Images," *International Journal of Computers and Their Applications*, vol. 10, pp. 185-197, 2003.

[3] B. Schefar and D. Casasent, "Non-linear Optical Hit-Miss Transform for Detection," *Applied Optics, Special Section on "Non-linear Techniques in Optical Pattern Recognition"*, vol. 34, p. 3869-3882, 1995.

[4] M. G. Löfdahl, M. J. v. Noort, and C. Denker, "Solar image restoration," *F. Kneer, K. G. Puschmann, and A. D. Wittmann, editors, Modern Solar Facilities - Advanced Solar Science. Universitätsverlag Göttingen, in press*, 2007.

[5] Koskinen, H., E. Tanskanen, R. Pirjola, A. Pulkkinen, C. Dyer, D. Rodgers, and P. Cannon, "Space Weather Effects Catalogue," *ESA Space Weather Programme Feasibility Studies, FMI, QinetiQ, RAL Consortium*, 2001.

[6] J. Tschirren, "Determination of the Envelope Function (Maximum Velocity Curve) in Doppler Ultrasound Flow Velocity Diagrams," University of Iowa, 2000.

[7] M. Zhang, K. Carder, F. MullerKarger, Z. Lee, and D. Goldgof, "Noise Reduction and Atmospheric Correction for Coastal Applications of Landsat Thematic Mapper Imagery," *Remote Sensing Environments*, vol. 70, pp. 167-180, 1999.

[8] M. Moore, M. Gabbouj, and S. Mitra, "Vector SD-ROM Filter for Removal of Impulse Noise from Color Images," in *Proceedings of the EURASIP, DSP for Multimedia Communications and Services (ECMCS)*, Krakow, 1999.

[9] M. Moore and S. Mitra, "Statistical threshold Design for the Two-State Signal Dependent Rank Order Mean Filter," in *Proc. IEEE International Conference on Image Processing (ICIP)*, Vancouver, 2000, pp. 904-907.

[10] J. Serra, *Image Analysis and Mathematical Morphology*. London: Academic press, 1982.

[11] P. Dong, "Implementaion of Mathematical Morphological Operations for Spatial Data processing," *Computers and Geosciences*, vol. 23, pp. 103-107, 1997.

[12] D. Casasent and B. Schefar, "Multilevel Hit-Miss Transform for Object Detection," in *Proceedings of SPIE*, Boston, 1994, pp. 2-9.

[13] C. Lee and S. Wong, "A Fuzzy Approach to Determine Morphological Thinning Algorithms for Fast Removal of Unwanted Skeletal Legs," *Engineering Application of Artificial Intelligence*, vol. 8, pp. 281-298, 1995.

[14] D. Casasent, "New Advances in Correlation Filters," in *Proceedings of SPIE Conference in Intelligent Robots and Computer Vision XI*, Pittsburgh, 1992, pp. 2-10.

[15] B. Schefar, D. Casasent, and A. Ye, "Optical Morphological Processors: Grey-scale With Binary Structuring Elements, Detection And Clutter Reduction," in *Proceedings of SPIE Conference in Intelligent Robots and Computer Vision XI*, Pittsburgh, 1992, pp. 427-442.

[16] R. Qahwaji and R. Green, "Hexagonal Hit-Miss Edge Detector," in *Proceedings of IEE CATEE-99*, Amman, 1999, pp. 278-281.

[17] R. Qahwaji and R. Green, "Detecting Objects in Digital Images," in *Proc. ISCA 16th International Conference on Computer Applications*, Seattle, 2001, pp. 15-19.

[18] NASA, How do we observe the Sun, http://soho.nascom.nasa.gov/explore/Sun_Obs.html, SOHO, last accessed: 2005.

[19] B. Poppe, A primer on space weather, http://gopher.sel.noaa.gov/primer/primer.html, last accessed: 2005.

[20] F. G. Eparvier, "Solar imaging needs for the space environment monitor on the Geostationary Operational Environmental Satellites (GOES R+)," Report of the GOES R Solar Imager Workshop, Laboratory for Atmospheric & Space Physics, University of Colorado, USA, 2001.